ACS Catalysis

Research Article

pubs.acs.org/acscatalysis

Rational Design of a Bifunctional Catalyst for the Oxydehydration of Glycerol: A Combined Theoretical and Experimental Study

Yang Sik Yun,[†] Kyung Rok Lee,[†] Hongseok Park,[†] Tae Yong Kim,[†] Danim Yun,[†] Jeong Woo Han,[‡] and Jongheop Yi*,[†]

[†]World Class University Program of Chemical Convergence for Energy and Environment, Institute of Chemical Processes, School of Chemical and Biological Engineering, Seoul National University, Seoul 151-742, Republic of Korea

[‡]Department of Chemical Engineering, University of Seoul, Seoul 130-743, Republic of Korea

Supporting Information

ABSTRACT: Due to its cost effectiveness and eco-friendliness, oxydehydration of glycerol is currently attracting considerable attention. In an attempt to develop an efficient catalyst for the reaction, tungsten-incorporated molybdenum vanadium mixed oxide (MoVW) catalysts were designed on the basis of computational calculations and mechanistic insights. By incorporating tungsten into molybdenum vanadium mixed oxide structure, the catalysts are active and selective not only for the dehydration of glycerol but also for the subsequent oxidation of acrolein to acrylic acid. Through DFT calculations, we confirmed that tungsten species induced a change in the electron density of neighboring atoms, which leads to selective production of acrylic acid. Structural characterization demonstrates that the structure of such MoVW catalysts is similar to that of DFT models. The incorporated tungsten species enhanced the acid and redox properties of the catalyst, leading to high selectivity for acrylic acid (30.5%). It not only induced but also stabilized the reduced oxidation states of molybdenum and vanadium atoms, as confirmed by XPS and DFT calculations. Hence, a stable and selective production of acrylic acid was achieved with full glycerol conversion for 110 h. The MoVW catalytic system with an additional acid catalyst bed exhibited remarkable selectivity for acrylic acid (47.2%), suggesting its potential for practical applications.

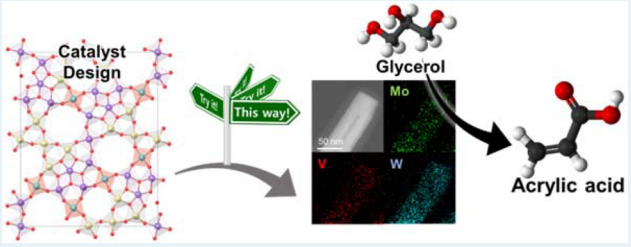

KEYWORDS: *catalyst design, bifunctional catalyst, glycerol, acrylic acid, density functional theory*

1. INTRODUCTION

Heterogeneous catalysts have played important roles in converting petroleum to fuel and fine chemicals over the past century.[1,2] Recently, due to depletion of fossil fuel combined with an increase in the price and the emergence of environmental problems, the utilization of biomass and its derivatives has been growing.[3−7] Hence, it is important to develop a new catalyst with high activity, selectivity, and stability for the production of fuels and valuable chemicals from biomass-based materials.

The oxydehydration of glycerol represents an alternative route to the petrochemical-based commercial process for the acrylic acid production. Acrylic acid is widely used as base material for paints, plastics, superabsorber polymers, and rubber synthesis.[8−10] The growing demand for plastics and superabsorbers in the polymer industry has stimulated intense interest in the sustainable production of acrylic acid.[10] The alternative reaction involves the sequential dehydration of glycerol to acrolein, followed by the selective oxidation of acrolein to acrylic acid.[8] This process faces several issues. For instance, multiple steps, which can lead to additional cost, workup, and waste generation, are involved.[11,12] Due to the high toxicity, volatility, and the reactivity of intermediates, especially acrolein, the handling of intermediates is difficult, and further isolation is required.[13,14] For the purpose of eliminating these limitations, therefore, the development of an integrated process using a bifunctional catalyst for the direct conversion of glycerol to acrylic acid is highly desirable.

A bifunctional catalyst for the direct conversion of glycerol to acrylic acid generally requires a combination of acid and selective oxidation properties without degradation of each active structure. However, the active structure (molybdenum vanadium mixed oxide) for the selective oxidation of acrolein is metastable, and it is easily influenced by pH and the metal concentration of the solution, the type of precursor, the activation process, and so forth.[10,15,16] Accordingly, a combination of two features with maintained intrinsic function is a significant challenge. In addition to a combination of two functions in one catalyst, it should possess suitable properties for each reaction. The first step, the dehydration reaction, proceeds in the presence of weak-to-medium acid strength acid sites.[17] For the selective oxidation of acrolein, the Mars−van

Received: September 1, 2014
Revised: November 10, 2014
Published: November 11, 2014

   dx.doi.org/10.1021/cs501307v | ACS Catal. 2015, 5, 82−94

Krevelen mechanism is widely accepted.[18] Based on this mechanism, unsaturated atoms with a high electron density and electronegativity act as adsorption sites for acrolein with an allylic intermediate being formed.[19,20] A nucleophilic and weakly bonded lattice oxygen on the catalyst surface is necessary for C−H activation and the selective insertion of oxygen into the intermediate.[21,22] In addition, it has been reported that vanadium as a redox center showing V^{4+} favors the selective oxidation of acrolein by stabilizing the oxygenated species in the form of acrylate.[20,23]

Despite the importance and necessity of bifunctional catalyst for the oxydehydration of glycerol, only a few catalysts have been developed for the direct conversion of glycerol to acrylic acid owing to the above complexity of requirements for bifunctional catalyst.[24−29] Although some of the catalysts have been somewhat successful from the standpoint of performance, there has been scant discussion on the fundamental understanding about active properties of catalysts and their relations to catalytic activity. As a result, time- and labor-consuming "trial-and-error" processes would be involved again in the development of new catalysts with better performance.[30]

Density functional theory (DFT) can be used to provide information regarding the mechanism of heterogeneous catalysis and the intrinsic properties of materials.[31−33] In addition, advancements made in computational power and accuracy now provide a platform for catalyst design based on extensive computational screening.[1,34] Several studies have achieved success in catalyst design at the atomic level through model prediction by DFT calculations and experimental demonstration.[35−37] Taking this into account, a combination of innovative computational calculations with accumulated knowledge can permit a catalyst with a high performance to be designed efficiently.

Herein, we report on tungsten-incorporated molybdenum vanadium mixed oxide (MoVW) catalysts as effective bifunctional catalysts for the direct conversion of glycerol to acrylic acid. Tungsten can be a good candidate as an acidic material to be combined with molybdenum vanadium mixed oxide (MoV) because it can work as a structure promoter.[10,17,38] The concept of incorporating an acidic tungsten species into the molybdenum vanadium mixed oxide framework allows the catalyst to be active and selective for both the dehydration of glycerol to acrolein and the subsequent oxidation of acrolein to acrylic acid. We initially employed DFT calculations to investigate the effect of tungsten on the electron density of neighboring atoms. The calculations were then confirmed by experiments. Finally, activity and stability tests were tested in single-bed and two-bed systems to confirm the enhanced catalytic behavior of the MoVW catalysts compared to MoV catalyst for the oxydehydration of glycerol. These comprehensive experiments, accompanied by DFT calculations, revealed the origin of enhanced catalytic performance of the catalyst. To the best of our knowledge, this is the first report of the use of a combination of experimental and theoretical studies for developing an efficient catalyst in this research area.

2. METHODS

2.1. Catalyst Preparation. Ammonium molybdate hydrate (99.0%, Samchun), vanadium oxide sulfate hydrate (97.0%, Sigma-Aldrich), ammonium metatungstate hydrate (99.0%, Sigma-Aldrich) were utilized as the metal precursor. Oxalic acid (98.0%) was purchased from Aldrich. All precursors were used without further purification.

MoVW samples were prepared by a hydrothermal method. Ammonium molybdate hydrate (7.06 g, 40 mmol) and 2.54−22.85 g (10−90 mmol) of ammonium metatungstate were dissolved in deionized water (96 mL). A stirred solution including 2.53 g (10 mmol) of vanadium oxide sulfate hydrate and deionized water (96 mL) was added to prepared solution. The mixture was stirred for an additional 10 min, and its pH value was then adjusted to 2.2 with 9 vol % aqueous sulfuric acid solution. The resulting solution was loaded into a glass-lined autoclave (real volume: 240 mL) and heated at 175 °C for 48 h. The solid product was separated from the solution by filtration, washed with deionized water, and dried at 80 °C overnight. The prepared samples were heat-treated in N_2 stream (50 mL/min) at 500 °C for 2 h. The final catalysts are referred to as MoVW-X where X indicates the molar ratio of tungsten compared to vanadium in preparation solution.

Reference samples, molybdenum vanadium mixed oxide (MoV) and tungsten oxide (WO_3), were also prepared according to previous reports.[26,39] In a typical experiment, 7.06 g of ammonium molybdate hydrate dissolved in 96 mL of deionized water was mixed with 2.53 g of vanadium oxide sulfate hydrate dissolved in 96 mL of deionized water. The mixture was stirred for 10 min, followed by adjustment of the pH value to 2.2 with aqueous sulfuric acid solution (9 vol %). The resulting solution was transferred to a glass-lined autoclave, and heated at 175 °C for 20 h. In the case of WO_3, an aqueous solution of ammonium metatungstate hydrate with oxalic acid (molar ratio of oxalic acid to W = 3) was located in a glass-lined autoclave, and the solution was heated at 175 °C for 48 h. Both samples were recovered by filtration, washed with deionized water, and dried at 80 °C overnight. The dried powdery samples of MoV and WO_3 were calcined in a stream of N_2 at 400 °C for 4 h and at 600 °C for 2 h, respectively.

2.2. Characterization. Ultraviolet−visible (UV−vis) spectra were recorded with a Jasco V670 spectrometer. The measurements were performed at 200−1000 nm in ambient atmosphere with 200 times diluted samples. XRD patterns of the catalysts were measured by using a Rigaku d-MAX2500-PC powder X-ray diffractometer operating at 50 kV and 100 mA using Cu Kα radiation (1.5406 Å). High-resolution transmission electron micrograph (HR-TEM) images were obtained on JEOL JEM-3010 microscope with an acceleration voltage of 300 kV. High-angle annular dark field scanning transmission microscopy (HAADF-STEM) image and corresponding elemental mapping images were acquired by means of FEI Tecnai F20 instrument equipped with an X-ray energy dispersive spectrometer. The specific surface areas of the samples were determined by N_2 adsorption at −196 °C, using the multipoint BET analysis method, with a Micromeritics ASAP-2010 system. The elemental compositions of the samples were determined by electron probe microanalysis (EPMA) using a JEOL JXA-8900R spectrometer. FT-IR spectra were obtained on a Nicolet 6700 (Thermo Scientific) FT-IR spectrophotometer in the range of 500−1100 cm^{-1}. The powdery samples were mixed with KBr (0.6 wt %) and pressed into translucent disks at room temperature. Raman spectroscopy was performed on a HORIBA Jobin Yven US/HR-800 using a multichannel charge-coupled device (CCD) detector at room temperature. The external laser source was used for excitation, a He−Ne laser at 632.8 nm. X-ray absorption spectroscopy (XAS) was carried out in transmission mode at the 8C nano XAFS beamline of Pohang Light Source (PLS) in the 3.0 GeV storage ring, with a ring current of 70−100 mA. A

dx.doi.org/10.1021/cs501307v | ACS Catal. 2015, 5, 82−94

Si (111) double-crystal was used to monochromatize the X-ray photon energy. Ionic chambers filled with N_2 (95%)/Ar (5%) and Ar (100%) were used for the I_0 and I detectors, respectively, at the W L_1-edge region. The samples were located between the ion chambers. Energy calibration of the W L_1-edge was carried out using Au foil. X-ray absorption near edge structure (XANES) spectra were recorded for each sample at room temperature using an energy step of 0.2 eV. The obtained data were normalized by Athena software.[40]

The NH_3 temperature-programmed desorption (NH_3-TPD) profiles were measured on a Micromeritics Autochem II chemisorption analyzer. A 0.1 g sample loaded in a U-shaped quartz reactor was pretreated in a He flow (50 mL/min) at 200 °C for 1 h and then cooled to room temperature. The samples were then exposed to a NH_3 gas mixture (10. 3% NH_3/He, 50 mL/min) and kept at 50 °C for 1 h for adsorption. The NH_3 that was physisorbed to the sample was eliminated by a flow of He (50 mL/min) at 100 °C for 30 min. NH_3-TPD profiles were obtained in a He flow (50 mL/min) by heating up to 500 °C at a rate of 10 °C/min. The desorbed NH_3 was measured by means of a thermal conductivity detector (TCD). X-ray photoelectron spectroscopy (XPS) was performed with a Sigma Probe instrument (ThermoVG). The binding energy of each element was calibrated by using the carbon peak as standard (C 1s = 284.5 eV). Peak assignment for each oxidation state of elements was conducted referring to previous researches.[41−44] The reducibility of the catalysts was studied by H_2 temperature-programmed reduction (H_2-TPR) experiments performed in a gas flow system measured by means of an online mass spectrometer (QGA, Hiden Analytical). The catalyst sample (50 mg) was placed in a U-shaped quartz reactor and pretreated in flowing Ar at 200 °C for 2 h, followed by cooling at room temperature. The temperature was then raised from room temperature to 700 °C with a heating rate of 10 °C/min in a 10% H_2/Ar flow (50 mL/min). The main (m/z) fragments registered were H_2 = 2 and Ar = 40.

2.3. Catalytic Activity Test. The catalytic activity tests were carried out at atmospheric pressure in the temperature range from 250 to 350 °C. A 0.3 g powder sample was loaded into a quartz reactor (8 mm inner diameter), and the reactor was then placed in an electric furnace. The temperature of the catalyst bed was monitored by a thermocouple and controlled through a PID controller. Before the reaction, the catalyst was preheated to the reaction temperature under an inert (He and N_2) flow (27.5 and 2.93 mL/min) for 1 h. A 1.2 M aqueous solution of glycerol was vaporized at a rate of 2 mL/h using a syringe pump. The vaporized reactant solution was diluted with a mixture of He, N_2, O_2 flow at the vaporizer and then fed into the catalyst bed. The molar composition of the reaction mixture used was [glycerol/O_2/H_2O/N_2/He] = [1.3/2.6/55.1/37.0/3.9]. The reaction products were passed through a condenser, and then collected in a cold trap that contained 20 mL of water and 1 mL of a 2 M 1-propanol aqueous solution. The collected products were analyzed by a gas chromatograph (Younglin ACME 6500 model) equipped with a FID detector and a HP-Innowax capillary column. 1-Propanol was used as internal standard for analyzing the liquid-phase products. The gaseous products were analyzed by an online GC (Younglin ACME 6000 model) equipped with a TCD detector and a Supelco Carboxen 1000 column. N_2 was used as internal standard for analyzing the gas-phase products. Glycerol conversion and product selectivity were calculated as follows:

$$\text{Glycerol conversion (\%)} = \frac{\text{mole of glycerol reacted}}{\text{mole of glycerol fed}} \times 100$$

$$\text{Yield (\%)} = \frac{\text{mole of product}}{\text{mole of glycerol fed}} \times \frac{C_i}{3} \times 100$$

$$\text{Selectivity (\%)} = \frac{\text{mole of product}}{\text{mole of glycerol reacted}} \times \frac{C_i}{3} \times 100$$

where C_i represents the number of carbon atoms of i product.

Carbon balance was calculated by summing up the unreacted glycerol and the total amount of detected products. Carbon balances were below 100% in each run because minor and heavy products with uncertain quantity were included, some product might be decomposed during analysis in chromatograms, and some volatile product might be missed in the condensing part.

2.4. DFT Calculations. The Vienna Ab-initio Simulation Package (VASP) was used for density functional theory (DFT) calculations.[45] We employed the generalized gradient approximation (GGA) parametrized by the Perdew−Burke−Ernzerhof (PBE) exchange−correlation functional.[46] Ionic cores were described by the projector augmented wave (PAW) method.[47] The wave functions were constructed from the expansion of planewaves with an energy cutoff of 520 eV. A 1 × 1 × 4 Monkhorst−Pack k-point mesh was used to sample the Brillioun zone. The self-consistent iterations were converged within a criterion of 4×10^{-4} eV, and the ionic optimization steps were converged to 0.03 eV/Å. Atomic charge analysis was performed using a Bader charge analysis.[48]

Equation 1 and 2 are our definitions of the substitutional (E_S) and interstitial incorporation energy (E_I) of tungsten atom, respectively:

$$E_S = (E_{\text{W sub-MoV}} + E_{\text{Mo or V}}) - (E_{\text{MoV}} + E_{\text{W}}) \quad (1)$$

$$E_I = (E_{\text{W inter-MoV}}) - (E_{\text{MoV}} + E_{\text{W}}) \quad (2)$$

where $E_{\text{W sub-MoV}}$ is the bulk energy of the MoV unit cell in which tungsten atom is substituted for molybdenum or vanadium atom, $E_{\text{W inter-MoV}}$ is the bulk energy of the MoV unit cell in which tungsten atom is interstitially inserted into the MoV structure, $E_{\text{Mo, V, or W}}$ is the bulk energy of the corresponding metal per atom, and E_{MoV} is the bulk energy of the MoV unit cell. More negative value of E_S and E_I means that the system is in the more stable state.

In order to evaluate the charge transfer by introducing tungsten, charge difference density was calculated using eq 3.[49,50]

$$\Delta\rho = \rho_{\text{MoVW}} - (\rho_{\text{MoV}} + \rho_{\text{W}}) \quad (3)$$

where ρ_{MoVW} is the total charge density of the MoVW system, ρ_{MoV} and ρ_{W} are the charge density of the system without tungsten and the isolated tungsten atoms, which are placed at the same atomic position as in the MoVW system. From the equation, variations in charge induced by interaction between host and foreign systems can be obtained by subtracting noninteraction systems from interaction system.

3. RESULTS AND DISCUSSION

3.1. Modeling of Tungsten Incorporated MoV Catalyst by DFT. Incorporating tungsten species into the MoV structure would facilitate dehydration of glycerol because tungsten oxide is well-known as an effective acid catalyst. However, it is hard to

dx.doi.org/10.1021/cs501307v | ACS Catal. 2015, 5, 82−94

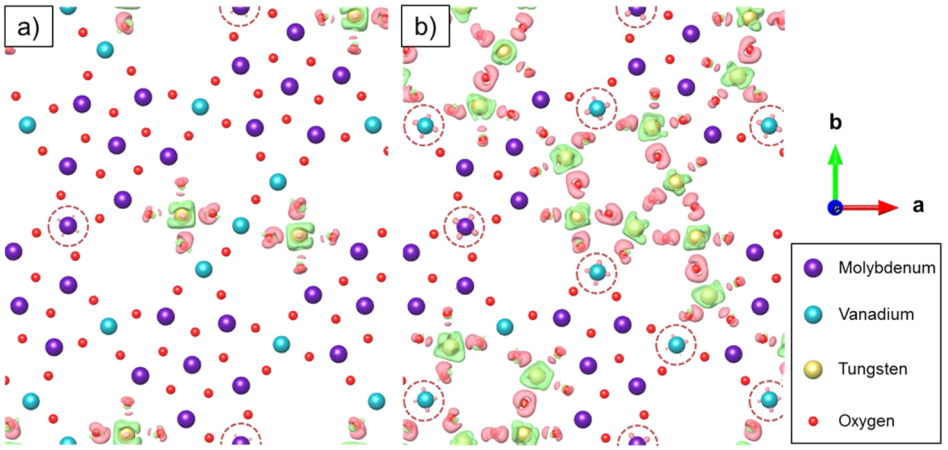

Figure 1. Calculated charge density differences for (a) MoVW-1 and (b) MoVW-5. Green color indicates a loss of electrons while pink shows a gain of electrons. Isosurface: 0.018.

expect the effect of the presence of tungsten on selective oxidation reaction before preparation and characterization of catalysts. Therefore, we introduced DFT calculations to confirm whether the desired properties for selective oxidation of acrolein to acrylic acid are derived by incorporating acidic tungsten species into the MoV structure.

To develop tungsten-incorporated molybdenum vanadium mixed oxide (MoVW) structure for DFT calculations, we attempted to identify the position of incorporated tungsten species in the MoV structure. To accomplish this, orthogonal MoV structure was first developed and optimized (Figure S1). We then calculated incorporation energies of tungsten into various positions in the MoV structure. The positions were chosen by considering the manner of incorporation (substitutional or interstitial incorporation) and the periodic nature of DFT calculations (Figure S1). Table S1 shows the DFT results for the substitutional (E_S) and interstitial (E_I) insertion energy of a tungsten atom at various positions calculated using eq 1 and 2. The E_S values were lower than E_I values, indicating that the substitutional incorporation of tungsten was more favorable than the interstitial incorporation of tungsten. In terms of the type of the substituted atom, the tungsten atom was thought to substitute in preference to the molybdenum atom rather than the vanadium atom. On the basis of the results of energy and probability calculations (Table S1–S4), we developed MoVW models (Figure S2), and possible configurations for each model were also listed in Table S5–S8. Details for modeling MoVW were discussed in Supporting Information.

Figure 1 and Figure S3 show charge transfer induced by introducing tungsten. The electrons were confirmed to transfer from a substituted tungsten atom to the surrounding oxygen, molybdenum, and vanadium atoms. Clearly, oxidation states of molybdenum and vanadium atoms were reduced, and lattice oxygen atoms around tungsten atoms became more nucleophilic due to a gain of electrons. Therefore, it was confirmed that by incorporating tungsten into MoV framework, the properties which are required for selective production of acrylic acid, such as abundance of reduced state of molybdenum and vanadium atoms as well as nucleophilic oxygen, were induced.[22,51]

Using Bader charge analysis, variation of oxidation state with different tungsten fraction was examined (Table 1). It was observed that tungsten atoms were present in a high oxidation state compared to molybdenum and vanadium atoms. The

Table 1. Average Oxidation State of Molybdenum, Vanadium, and Tungsten in MoV and MoVW Catalysts, Calculated by Bader Charge Analysis

	calcd oxidation state		
catalyst	Mo	V	W
MoV	+3.63	+2.58	
MoVW-1	+3.61	+2.58	+4.52
MoVW-3	+3.55	+2.56	+4.54
MoVW-5	+3.51	+2.50	+4.48
MoVW-7	+3.45	+2.50	+4.49

oxidation state of molybdenum and vanadium atoms was decreased with an increase in tungsten contents. This clearly demonstrates that tungsten induced a reduced state of redox center (vanadium)[52] and molybdenum. From this, it is expected that the catalysts with high tungsten content would exhibit high performance in acrylic acid production due to the most reduced oxidation state of vanadium among the catalysts. Consequently, by comprehensive DFT calculation, we confirmed the incorporated tungsten change intrinsic properties, which can lead to high selectivity to acrylic acid.

3.2. Structural Characterization. MoVW catalysts were verified as good candidates with high selectivity for acrylic acid production by using DFT calculations. Hence, we intended to develop real catalysts, which have similar structure with theoretical models, for validating the results experimentally. The catalysts with tungsten containing MoV structure were prepared by means of a hydrothermal reaction. In the synthetic mechanism via hydrothermal reaction, a pentagonal $(M)M_5O_{21}$ polyoxometalate unit (building block) is essential for formation of the molybdenum vanadium mixed oxide structure. UV–vis spectra were collected to confirm whether the building block is formed in the preparation solution even with the tungsten precursor (Figure S4). All of the spectra of the MoV and MoVW solutions showed a peak at around 510–550 nm, similar to that of $Mo_{72}V_{30}$ which consists of pentagonal polyoxomolybdate units connected with vanadium centered octahedrons.[16,53] From these results, the presence of the building block in the MoVW precursor solution even in the presence of a large amount of tungsten precursor is confirmed.

X-ray diffraction (XRD) was employed to investigate the crystalline structure of the MoV and MoVW catalysts, and the corresponding results are shown in Figure 2A. The MoV and

dx.doi.org/10.1021/cs501307v | ACS Catal. 2015, 5, 82–94

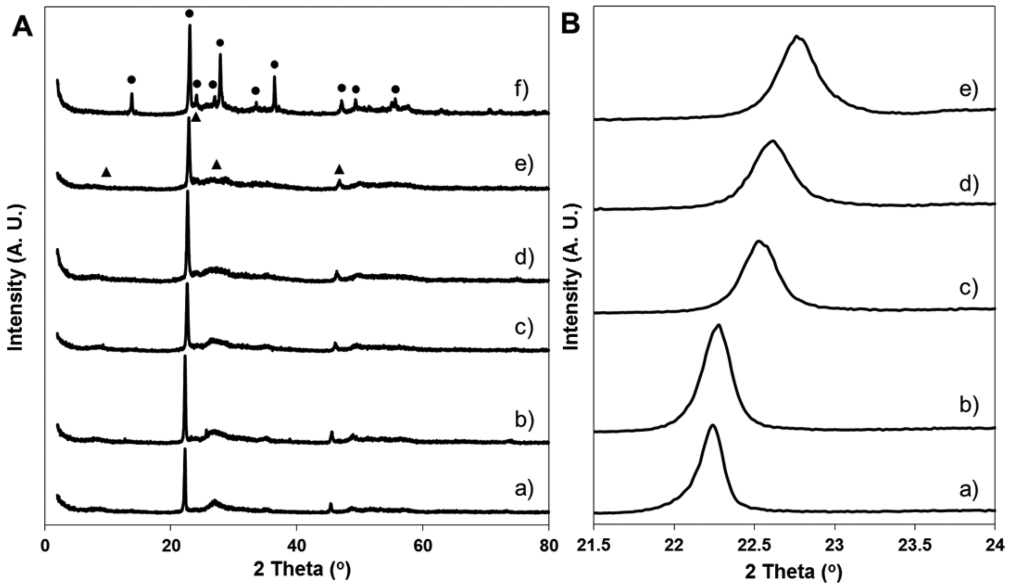

Figure 2. (A) XRD patterns of (a) MoV, (b) MoVW-1, (c) MoVW-3, (d) MoVW-5, (e) MoVW-7, and (f) MoVW-9 catalysts. (B) Effect of the amount of tungsten atoms on the shift in XRD patterns. ●: hexagonal tungsten bronze ▲: amorphous MoV.

MoVW catalysts (except for the MoVW-9 catalyst) exhibited the characteristic diffraction of amorphous molybdenum vanadium mixed oxide (amorphous MoV) structure[54] without any evidence for the presence of WO_x phase even in high levels of tungsten (MoVW-7). Therefore, it was confirmed that molybdenum vanadium mixed oxide structure containing tungsten species was successfully developed. The XRD patterns showed highly intense peaks at 2θ = 22° and 45°, and broad peaks at ca. 2θ = 10° and 26°, corresponding to layered structures with disordered slabs and an ordered layer distance along the [001] direction (*c*-direction), respectively.[54,55] Previous papers have reported that the unique structure are essential for the selective oxidation of acrolein to acrylic acid.[56] Accordingly, the catalysts are expected to be active and selective for the conversion of acrolein to acrylic acid.

The crystalline peak (2θ = 22°) was shifted to a higher angle with increasing tungsten content, while the structure was maintained (Figure 2B). This is clear evidence for incorporation of tungsten into the framework. Table 2 shows the theoretically and experimentally calculated lattice parameters along the c-direction. The both parameters showed a similar trend along tungsten fractions. This result clearly demonstrates as-prepared MoVW catalysts are well-synthesized as we designed by DFT-designed models.

Table 2. Experimental and Calculated Lattice Constant of [100] Direction (*c*-Direction) of MoV and MoVW Catalysts

	d (Å)	
catalyst	exptl (XRD)	calcd (DFT)
MoV	3.995	4.097
MoVW-1	3.991	4.071
MoVW-3	3.946	4.023
MoVW-5	3.934	3.984
MoVW-7	3.907	3.956

Unlike the trends for the crystalline peaks, the peaks around 2θ = 10° and 26° became broader with increasing tungsten content, indicating that the slab plane became more disordered. When the ratio of tungsten to vanadium reached 9, the catalyst no longer showed the unique structure of amorphous MoV but, rather, exhibited characteristic peaks corresponding to hexagonal tungsten bronze.[26] The reason for this, we suggest, is that the hexagonal tungsten bronze structure becomes thermodynamically more stable than the amorphous MoV structure in the preparation process as degree of irregularity of the *a*−*b* plane increases in the presence of a high content of tungsten.

The TEM images of MoVW showed that the samples are rod shaped with an average diameter in range of 20−40 nm as shown in inset of Figure 3. Magnified HR-TEM images confirmed that the MoVW-1 to 7 samples have a layered-type structure along the *c*-direction without other lattices such as WO_3 (Figure S5). This unique structure is analogous to the structure of crystalline MoV,[39] suggesting that the structure of MoV was maintained even in the presence of tungsten. Although exhibiting an ordered array along the *c*-direction, the lattice oriented parallel to the *c* axis appeared to show irregularity. These results suggest that the MoVW samples had a disordered *a*−*b* plane and a highly ordered layer distance of about 4 Å along the *c*-direction, which is consistent with the XRD results (Figure 2).

In order to examine the homogeneity of tungsten, high-angle annular dark field (HAADF) images and corresponding elemental mapping images of MoVW-1 and MoVW-5 were obtained (Figure 4). Molybdenum, vanadium, and tungsten atoms were homogeneously dispersed throughout the MoVW-1 and MoVW-5 catalysts. This clearly indicates that no phase separation occurred, regardless of the magnitude of the tungsten fraction in the samples.

To further investigate the structure of MoVW catalysts, FT-IR and Raman analyses were conducted (Figure S6). In the case of MoV catalyst, peaks at 915 cm^{-1} for V═O, 870 cm^{-1} for Mo═O, 652, 716, 917 cm^{-1} for Mo−O−Mo, and 604 cm^{-1} for Mo−O−V were obtained in the FT-IR spectrum (Figure S6A). Similarly, sharp bands at 285, 819, 871, and 997 cm^{-1} attributed to Mo−O−Mo and Mo═O, respectively, were observed in Raman spectra (Figure S6B). These are in agreement with the

dx.doi.org/10.1021/cs501307v | ACS Catal. 2015, 5, 82−94

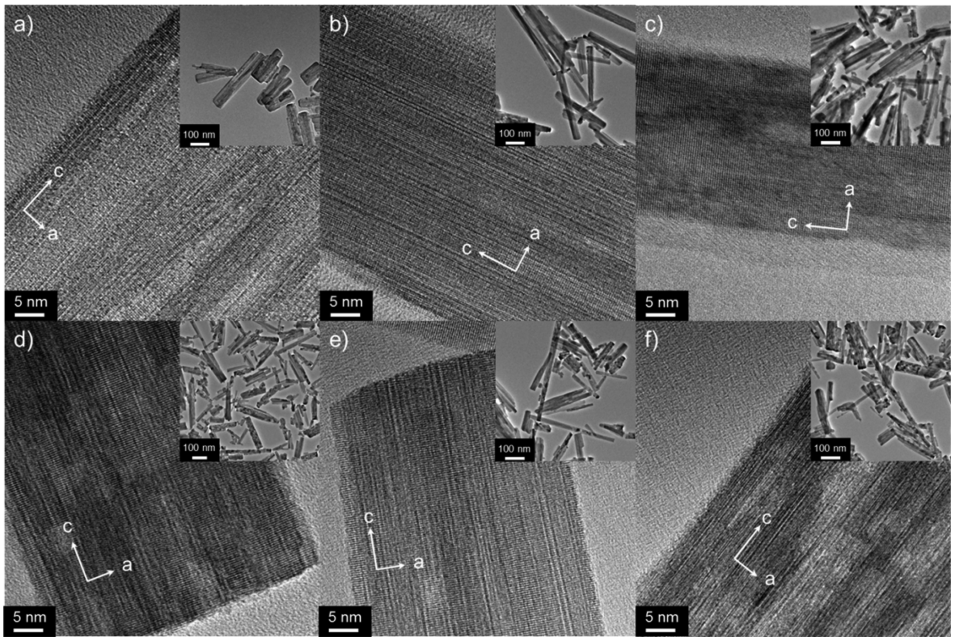

Figure 3. HR-TEM images of (a) MoV, (b) MoVW-1, (c) MoVW-3, (d) MoVW-5, (e) MoVW-7, and (f) MoVW-9 catalysts. Insets indicate low magnification images.

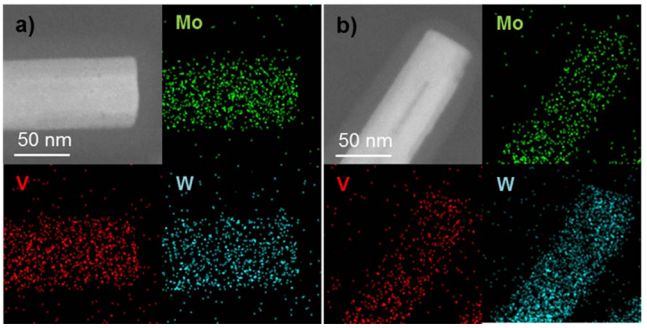

Figure 4. HAADF-STEM images of (a) MoVW-1, (b) MoVW-5, and their corresponding elemental mapping images of Mo (green), V (red), and W (sky blue).

characteristic peaks corresponding to a molybdenum vanadium mixed oxide.[51,54] However, a change was noted in the case of the tungsten-containing catalyst. Despite the small proportion of tungsten in the MoVW-1 catalyst (EPMA results in Table 3), the bands attributed to Mo═O and Mo−O−Mo were decreased considerably. Moreover, no additional peak corresponding to W−O−W bond (813−830 cm^{-1} in the FTIR spectra, and 273, 329, 720, and 809 cm^{-1} in Raman spectra) was observed.[26,57] These findings suggest that the tungsten species did not form a separate phase such as WO_3 but rather was incorporated into the MoV structure in substitutional manner. As the amount of tungsten in the catalysts became higher, peaks related to molybdenum−oxygen and vanadium−oxygen bonds became smaller while peaks arising from tungsten−oxygen bonds became dominant.

Figure 5 shows XANES spectra around the W L_1-edge region. The local geometry of tungsten can be determined by the pre-edge of the W L_1-edge region.[58] The pre-edge peak at the W L_1-edge, caused by a 2s →5d transition, shows a significant intensity in the case of tetrahedral symmetry while small or no peaks are obtained in octahedral symmetry.[58] The MoVW catalysts exhibited a small pre-edge peak in the W L_1-edge region, indicating that incorporated tungsten species have distorted octahedral units, which are the same tungsten coordinates with MoVW models (Figure S2). MoVW-1 showed a relatively distinct peak compared to a sample of the reference catalyst (WO_3). As the tungsten content increased, the peak became smaller, and analogous to that of WO_3. It was found that octahedrons in MoVW-1 were more distorted than that of the others, and the degree of distortion was decreased with

Table 3. Physicochemical Properties of the MoV and MoVW Catalysts

catalyst	specific surface area[a] (m^2/g)	acid amount[b] (mmol/g)	relative bulk compositions[c] (Mo/V/W)	surface compositions[d] (Mo/V/W/O)	crystal structure[e]
MoV	21.2	0.259	2.6/1.0/0.0	24.2/5.2/0.0/70.6	amorphous-MoVO
MoVW-1	22.8	0.260	2.4/1.0/0.4	19.1/3.4/7.9/69.6	amorphous MoVO
MoVW-3	36.8	0.438	2.8/1.0/1.4	15.1/2.4/12.3/70.2	amorphous MoVO
MoVW-5	25.0	0.485	3.2/1.0/2.5	12.3/1.7/16.1/70.0	amorphous MoVO
MoVW-7	22.2	0.321	3.0/1.0/3.4	10.0/1.4/18.0/70.5	amorphous MoVO
MoVW-9	17.4	0.270	3.0/1.0/5.6	7.7/1.1/19.3/71.9	hexagonal tungsten bronze

[a]Specific surface area was determined from the N_2 adsorption branch. [b]The amount of acid sites was evaluated on the basis of NH_3 temperature-programmed desorption (NH_3-TPD). [c]Elemental compositions of solid catalysts were determined by EPMA. [d]Surface composition was obtained by XPS analysis. [e]Crystalline structure was determined by XRD analysis.

dx.doi.org/10.1021/cs501307v | ACS Catal. 2015, 5, 82−94

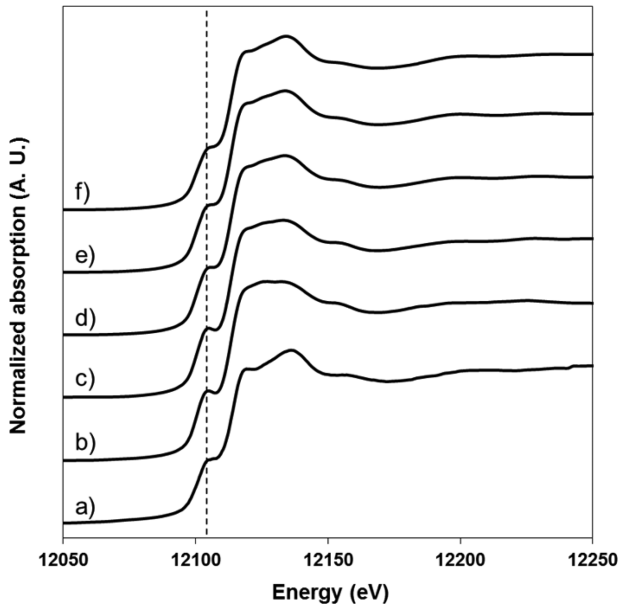

Figure 5. W L_1-edge XANES spectra of (a) WO_3, (b) MoVW-1, (c) MoVW-3, (d) MoVW-5, (e) MoVW-7, and (f) MoVW-9 catalysts.

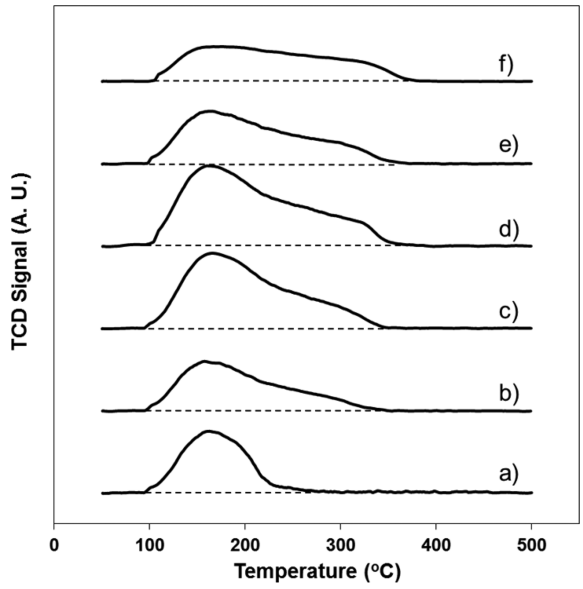

Figure 6. NH_3-TPD curves of (a) MoV, (b) MoVW-1, (c) MoVW-3, (d) MoVW-5, (e) MoVW-7, and (f) MoVW-9 catalysts.

increasing tungsten content. Combination with previous energetics for incorporation of tungsten, it is confirmed that tungsten was located at molybdenum or vanadium positions with octahedral coordinates in MoV structure.

3.3. Effect of Incorporated Tungsten on Acid and Redox Properties. The above findings clearly indicate that MoVW catalysts were successfully developed and that their structures were similar to those for models designed by DFT. It therefore appears that chemical interactions among molybdenum, vanadium, tungsten, and oxygen occur, as previously calculated. NH_3-TPD, XPS, and H_2-TPR were employed to investigate changes in the intrinsic properties of the samples, such as acid properties, the oxidation state of the metal components and lattice oxygen, which facilitates the dehydration of glycerol and the selective oxidation of acrolein.

NH_3-TPD analysis was performed to investigate the effect of tungsten on the acid properties of the sample. As shown in Figure 6 and Table 3, the MoVW catalysts were confirmed to possess a higher number of acid sites than the MoV catalyst (0.259 mmol/g). The amount of acid increased from MoVW-1 (0.260 mmol/g) to MoVW-5 (0.485 mmol/g) and then decreased from these values in MoVW-9 (0.270 mmol/g). Note that the NH_3 desorption peak was located below 200 °C in the MoV sample, suggesting a low acid strength. As tungsten was incorporated, additional shoulders around 300 °C appeared. This indicates that acid sites with a high acid strength were generated by the presence of tungsten. It can be attributed to the high electronegativity of tungsten compared to that of molybdenum and vanadium.[59] This enhancement in acid properties would enhance the conversion of glycerol to acrolein, the first step in the oxydehydration of glycerol.

To understand effect of incorporated tungsten on the oxidation state of molybdenum and vanadium atoms, the MoV and MoVW catalysts were investigated by means of an XPS technique. As shown in Table 4, for MoV sample, most of the molybdenum atoms were present in a high oxidation state (Mo^{6+}). Both V^{4+} and V^{5+} were observed in the catalyst, with a $V^{4+}/(V^{4+} + V^{5+})$ ratio of 0.667. The oxidation state of molybdenum and vanadium in the MoVW catalysts was significantly changed by the addition of tungsten. The ratio of $Mo^{5+}/(Mo^{5+} + Mo^{6+})$ was increased from 0 to 0.266 when the tungsten content increased. The $V^{4+}/(V^{4+} + V^{5+})$ ratio was also increased from 0.667 in the MoV catalyst to 0.750 in MoVW-5 and decreased to 0.694 in MoVW-9. In the case of tungsten atoms, oxidized species (W^{6+}) were dominant regardless of tungsten fraction. That is, when tungsten was incorporated into the MoV framework, Mo^{6+} and V^{5+} were reduced to Mo^{5+} and V^{4+} while tungsten ions were in an oxidized state (W^{6+}). Interestingly, the result that tungsten induces reduced states of molybdenum and vanadium in XPS, is good agreement with previous DFT calculation (charge density differences and Bader charge analysis). It demonstrates the validity of designed MoVW models by DFT. In comparison with results of Bader charge analysis (Table 1), a similar trend according to tungsten contents was obtained, except in the MoVW-7 catalyst. The reason for this, we suggest, is that MoVW-7 catalyst exhibited a more disordered $a-b$ plane than other catalysts due to high content of tungsten (Figure 2).

H_2-TPR was performed to study reducibility of the samples (Figure 7). The performance of a selective oxidation catalyst is closely related to the reducibility of the lattice oxygen in the catalysts.[60−62] A broad peak was observed for the MoV sample in the range of 450−650 °C. This can be attributed to complex molybdenum and vanadium mixed oxide species, not V_2O_5 and MoO_3.[63] Compared to the MoV sample, peaks of the MoVW samples were shifted toward lower temperatures. The peaks were not exactly defined, but it was certain that a weaker metal−oxygen interaction was induced as the result of the incorporation of tungsten into MoV framework. That is to say, tungsten-containing samples were able to easily release solid oxygen species, resulting in the highly selective conversion of acrolein to acrylic acid.

3.4. Effects of Reaction Temperature and Contact Time on Activity. The dehydration of glycerol is an endothermic reaction, whereas the oxidation of acrolein is an exothermic reaction.[25] In addition, the two reactions have different optimal reaction temperature.[8] Accordingly, it is worthwhile to trace product distributions over bifunctional

dx.doi.org/10.1021/cs501307v | ACS Catal. 2015, 5, 82−94

Table 4. Oxidation State of Molybdenum, Vanadium, and Tungsten in MoV and MoVW Catalysts before and after Reaction[a]

	before reaction			after reaction[b]		
catalyst	$Mo^{5+}/(Mo^{5+} + Mo^{6+})$	$V^{4+}/(V^{4+} + V^{5+})$	$W^{5+}/(W^{5+} + W^{6+})$	$Mo^{5+}/(Mo^{5+} + Mo^{6+})$	$V^{4+}/(V^{4+} + V^{5+})$	$W^{5+}/(W^{5+} + W^{6+})$
MoV	0.000	0.667		0.000	0.599	
MoVW-1	0.000	0.674	0.019	0.007	0.660	0.016
MoVW-3	0.084	0.695	0.042	0.091	0.691	0.005
MoVW-5	0.234	0.750	0.051	0.230	0.740	0.015
MoVW-7	0.260	0.712	0.038	0.232	0.679	0.000
MoVW-9	0.266	0.694	0.082	0.255	0.668	0.062

[a]Binding energy: Mo^{5+} ($3d_{5/2}$ = 231.7 ± 0.2 eV, $3d_{3/2}$ = 234.8 ± 0.2 eV), Mo^{6+} ($3d_{5/2}$ = 232.8 ± 0.2 eV, $3d_{3/2}$ = 235.9 ± 0.2 eV), V^{4+} ($2p_{3/2}$ = 516.7 ± 0.2 eV), V^{5+} ($2p_{3/2}$ = 517.7 ± 0.2 eV), W^{5+} ($4f_{7/2}$ = 35.0 ± 0.2 eV, $4f_{5/2}$ = 37.1 ± 0.2 eV), W^{6+} ($4f_{7/2}$ = 35.6 ± 0.2 eV, $4f_{5/2}$ = 37.7 ± 0.2 eV). [b]Reaction conditions: catalyst amount 0.3 g; reaction temperature 250 °C; total feed rate 74.34 mL min^{-1}; feed composition (vol %) glycerol/O_2/H_2O/N_2/He = 1.3/2.6/55.1/37.0/3.9. The catalysts were collected after 14 h time-on-stream reaction.

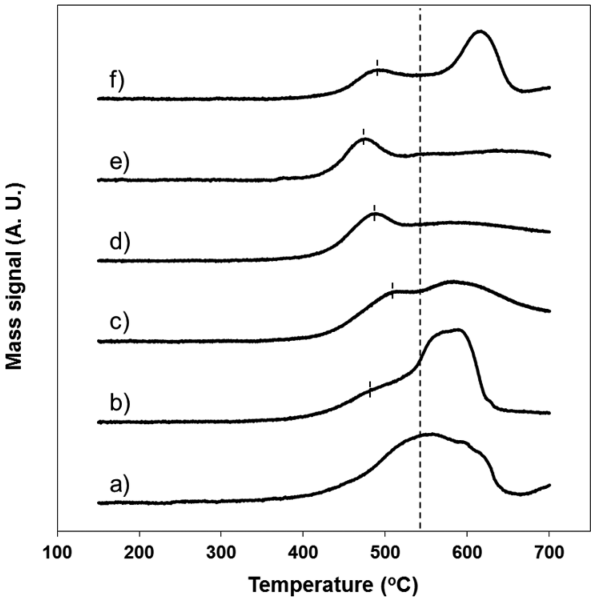

Figure 7. H_2-TPR curves of (a) MoV, (b) MoVW-1, (c) MoVW-3, (d) MoVW-5, (e) MoVW-7, and (f) MoVW-9 catalysts.

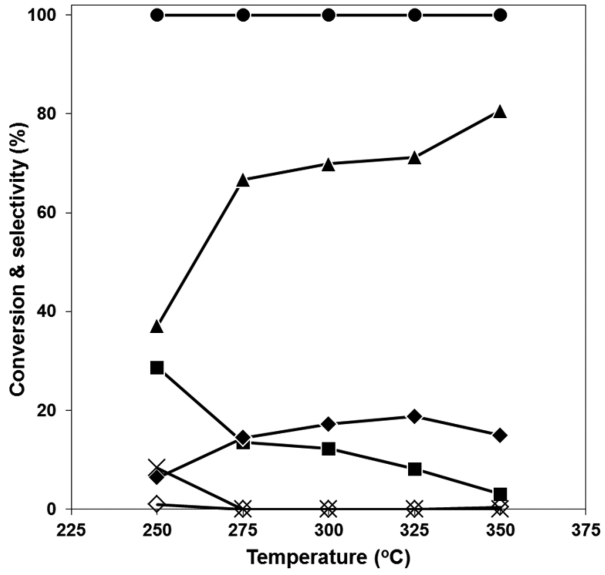

Figure 8. Glycerol conversion (●) and product selectivities (▲: CO + CO_2; ■: acrylic acid; ◆: acetic acid; ×: acrolein; and ◇: acetaldehyde) in oxydehydration of glycerol over MoVW-5 catalyst as a function of reaction temperature. Reaction conditions: catalyst amount 0.3 g; total feed rate 74.34 mL min^{-1}; feed composition (vol %) glycerol/O_2/H_2O/N_2/He = 1.3/2.6/55.1/37.0/3.9. The reaction results were taken after 3 h time-on-stream.

catalyst as a function of reaction temperature. Figure 8 shows catalytic test results for different reaction temperatures. The conversion of glycerol was complete over the range of temperatures used. It is still worth comparing product selectivities in full conversion of glycerol because it is consecutive reactions.[64] The highest selectivity for acrylic acid was observed at 250 °C. When the reaction temperature reached 275 °C, the selectivity for acrylic acid was reduced by more than half (13.5%). In addition, primary products (acetaldehyde, acrolein, etc.) were rarely detected. The results imply that reactant and products were unselectively oxidized to CO and CO_2 (66.7%) at high reaction temperature. A further increase in temperature from 275 to 350 °C led to a progressive decline in selectivity for acrylic acid (ca. 3%) and a significant increase in CO_x up to 80.7%. The higher selectivity for acetic acid could be the result of the oxidation of acetaldehyde and the cleavage of the C−C bond of acetol and acrylic acid by activation of acid sites, respectively, at temperatures higher than 250 °C.[65]

Generally, in a long contact time, acrolein production from glycerol is facilitated over acid sites, whereas selectivity from acrolein to acrylic acid is decreased over oxidation sites. On the other hand, in the case of a short contact time, the opposite tendency was observed.[66,67] Hence, the contact time not only of the reactant (glycerol) but also the intermediate (acrolein) should be optimized for the acrylic acid production. The effect of contact time on the product distribution of glycerol oxydehydration over the MoVW-5 catalyst was investigated at 250 °C (Figure 9). The test was performed with varying amounts of catalyst with the same feed rate. Even at a short contact time (0.05 s), the conversion of glycerol was complete. Primary products (acrolein and acetaldehyde), secondary products (acrylic acid and acetic acid), and total oxidation products (CO and CO_2) were detected. When the contact time reached 0.16 s, selectivity for acrylic acid increased from 22.2% to 28.7%, and CO_x production was decreased from 42.5% to 37.1% compared to contact time of 0.05 s. This result suggests that there is a lack opportunity for reactants and intermediates to come into contact with acid sites and oxidation sites, respectively, at a short contact time, which can stimulate undesired reaction to produce byproducts. On the other hand, at a contact time of 0.16 s, as the dehydration of acrolein and the consecutive selective oxidation of acrolein were balanced, a high yield of acrylic acid with a low yield of byproducts were

dx.doi.org/10.1021/cs501307v | ACS Catal. 2015, 5, 82−94

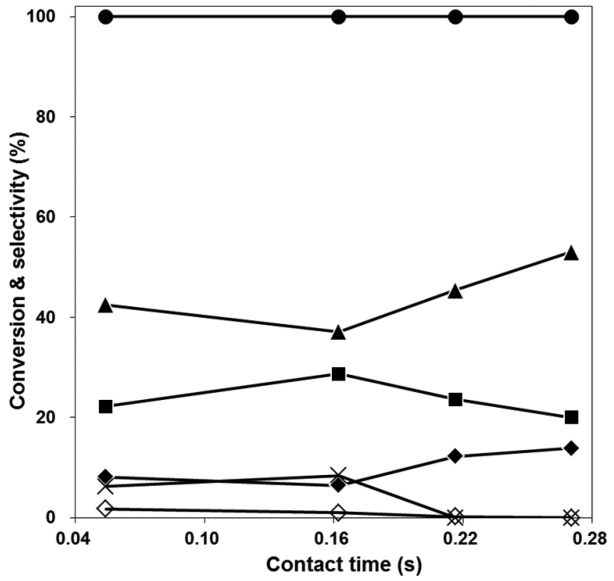

Figure 9. Glycerol conversion (●) and product selectivities (▲: CO + CO_2; ■: acrylic acid; ◆: acetic acid; ×: acrolein; and ◇: acetaldehyde) in oxydehydration of glycerol over MoVW-5 catalyst as a function of contact time. Reaction conditions: reaction temperature 250 °C; total feed rate 74.34 mL min^{-1}; feed composition (vol %) glycerol/O_2/H_2O/N_2/He = 1.3/2.6/55.1/37.0/3.9. The reaction results were taken after 3 h time-on-stream.

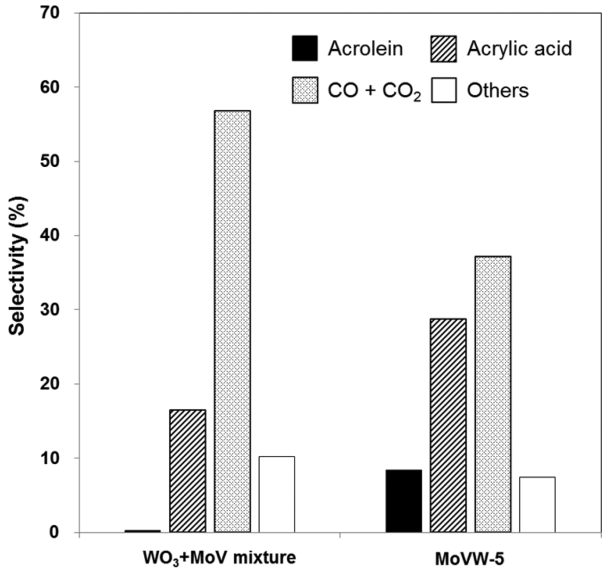

Figure 10. Comparative study of physically mixed WO_3 and MoV catalysts, and MoVW-5 catalyst in oxydehydration of glycerol. Reaction conditions: MoVW-5 0.3 g; reaction temperature 250 °C; total feed rate 74.34 mL min^{-1}; feed composition (vol %) glycerol/O_2/H_2O/N_2/He = 1.3/2.6/55.1/37.0/3.9. The reaction results were taken after 3 h time-on-stream. Mixed system: WO_3 0.1646 g, MoV 0.135 g. Others include acetaldehyde and acetic acid.

observed. As the contact time was increased (>0.2 s), selectivity for CO_x significantly increased, reaching 53.1% at 0.27 s, and the selectivity for acrylic acid was simultaneously decreased. Primary products were not observed and acetic acid was increased. Considering the results, the increased chance to contact reactant and products with vanadium species, well-known as redox sites,[52] stimulates the transformation of primary products into secondary product and enhances the total oxidation of products.

3.5. Effect of Tungsten on Catalytic Activity for Oxydehydration of Glycerol. To clarify the effect of incorporated tungsten on catalytic performance for the oxydehydration of glycerol, we compared the physically mixed catalyst (WO_3 and MoV) and MoVW-5. WO_3 was prepared by the same procedure as previously reported, showing a high yield of acrolein.[26] To load the physically mixed catalysts with the same moles of molybdenum, vanadium, and tungsten corresponding to 0.3 g of MoVW-5 catalyst, we calculated the weight of the WO_3 and MoV catalysts based on EPMA results (Table 3). Figure 10 shows the results for the oxydehydration of glycerol over both catalytic systems. Full conversion and a similar yield of acetaldehyde and acetic acid (denoted "others") were obtained in both systems. However, the selectivity for acrylic acid over MoVW-5 was almost twice as that over the WO_3 and MoV mixture. In addition, much lower production of CO_x was observed over MoVW-5 compared to the physical mixture of WO_3 and MoV catalysts. If a separate phase of MoV and WO_x was formed in MoVW-5, the reaction results would be similar to a physical mixture system. From this, we clarified that tungsten species are incorporated into the MoV framework, thus enhancing acid and redox properties. It was also found that total oxidation was suppressed by the presence of tungsten, resulting in an enhancement in selectivity for acrylic acid.

The catalytic performance for the oxydehydration of glycerol over the MoVW catalysts with different tungsten fractions is presented in Table 5. For comparison, MoV catalyst without tungsten was also tested. Full glycerol conversion was obtained over all of the catalysts. The catalyst without tungsten (MoV) exhibited extremely high selectivity for CO_x (66.2%) with a low production of acrylic acid (12.4%). Over the MoVW-1 catalyst, although even a small amount of tungsten was present, selectivity for acrylic acid was significantly increased from 12.4% to 21.7%. Products corresponding to the complete oxidation (CO_x) were also remarkably decreased from 66.2% to 50.9%. In addition, unconverted acrolein was obtained in contrast to the results for MoV catalyst. The physicochemical properties of the MoVW-1 catalyst, such as surface area, acid amounts, and crystal structure, were similar to those for the MoV catalyst (Table 3). The main differences were the oxidation state of metal atoms and reducibility. Taking this account, the high reducibility and the reduced oxidation state of metal atoms caused by the incorporation of tungsten are reasons why the MoVW-1 catalyst showed higher selectivity for acrylic acid than MoV catalyst.

As the tungsten content in MoVW catalysts was increased, the selectivity of acrylic acid was increased from MoVW-1 (21.7%) to MoVW-5 (30.5%) with a significant decrease in CO_x production (35.6%). With a further increase in the tungsten fraction to MoVW-7, CO_x selectivity was slightly increased, whereas acrylic acid selectivity was decreased. In the case of MoVW-9, with hexagonal tungsten bronze structure (Figure 2), selectivity for acrylic acid (12.6%) was comparable with that of the MoV catalyst. In addition, large amounts of unconverted acrolein and acetaldehyde were observed, indicating that its characteristic structure (hexagonal tungsten bronze) is less active for the selective oxidation than the MoV phase. This suggests that the MoV phase is necessary for the efficient conversion of acrolein to acrylic acid in glycerol

dx.doi.org/10.1021/cs501307v | ACS Catal. 2015, 5, 82−94

Table 5. Conversion and Selectivities of MoV and MoVW Catalysts with Various Tungsten Contents[a]

		selectivity (%)				
catalyst	glycerol conversion (%)	acrylic acid	acrolein	acetic acid	CO_x	acetaldehyde
MoV	100	12.4	0.0	8.6	66.2	<1.0
MoVW-1	100	21.7	2.0	8.4	50.9	<1.0
MoVW-3	100	23.2	2.1	8.8	48.0	<1.0
MoVW-5	100	30.5	8.2	8.5	35.6	3.3
MoVW-7	100	21.3	9.4	7.0	38.7	3.6
MoVW-9	100	12.6	20.0	5.6	34.6	5.6

[a]Reaction conditions: catalyst amount 0.3 g; reaction temperature 250 °C; total feed rate 74.34 mL min^{-1}; feed composition (vol %) glycerol/O_2/H_2O/N_2/He = 1.3/2.6/55.1/37.0/3.9. The reaction results were taken after 14 h time-on-stream.

oxydehydration, and the maintenance of its structure even with incorporation of tungsten is crucial for functioning as an efficient bifunctional catalyst.

For a clear understanding of product variation with different compositions, the total yield of acrolein and acrylic acid, acid amounts, selectivity of CO_x in oxidation products, and ratios of $V^{4+}/(V^{4+} + V^{5+})$ were plotted as a function of tungsten content (Figure 11). To exclude the effect of structure, catalysts with MoV structure were included (MoVW-1 to 7). Acid amount exhibited a similar trend of total production of acrolein and acrylic acid along with tungsten content and also showed a maximum peak at the same tungsten content of 5 (Figure 11A). Hence, high acid density can be advantageous for producing acrylic acid, confirming acrylic acid is produced from glycerol via acrolein.[8,26] In Figure 11B, we used "selectivity in oxidation products (acrylic acid, acetic acid, and CO_x)" to clarify influence of oxidation states of vanadium atoms on oxidation product distributions. As the tungsten content increased, the ratio of $V^{4+}/(V^{4+} + V^{5+})$ was increased to MoVW-5 and decreased to MoVW-7. Interestingly, an opposite trend was obtained in a plot of CO_x selectivity in oxidation products with tungsten content. This indicates that the ratio of $V^{4+}/(V^{4+} + V^{5+})$ is a crucial determinant of selectivity for acrylic acid and CO_x, and V^{4+} is favorable for converting acrolein into acrylic acid rather than CO_x. Consequently, it was confirmed that high acid properties and ratio of $V^{4+}/(V^{4+} + V^{5+})$ of MoVW-5 catalyst resulted in the highest selectivity for acrylic acid among the catalysts tested. Furthermore, it is obvious that introduced tungsten played a role not only as an acidic species but also as a promoter to suppress total oxidation by reducing the vanadium species.

3.6. Effect of Tungsten on Catalytic Stability of MoVW Catalyst. For an investigation of the effect of tungsten on the stability of the MoVW catalyst, XPS analysis and long-term catalytic tests were carried out. In previous research, the deactivation of bifunctional catalysts was mainly reported to be caused by a change in the oxidation state of the redox center rather than acid sites.[26] To address this issue, we employed XPS analysis to compare the oxidation state of metal atoms in MoV and MoVW catalysts before and after the reactions (Table 4). For both MoV and MoVW catalysts, vanadium atoms were oxidized after the reaction while other metal ions were rarely changed. This suggests that vanadium works as a redox center. In MoV catalyst, the ratio of $V^{4+}/(V^{4+} + V^{5+})$ was decreased remarkably from 0.667 to 0.599. On the other hand, only a small portion of V^{4+} was oxidized to V^{5+} in the MoVW catalysts. Instead, molybdenum and tungsten were slightly oxidized. That is, V^{4+} was stabilized in the presence of tungsten species. This can result in a high catalytic stability of MoVW catalysts for oxydehydration of glycerol.

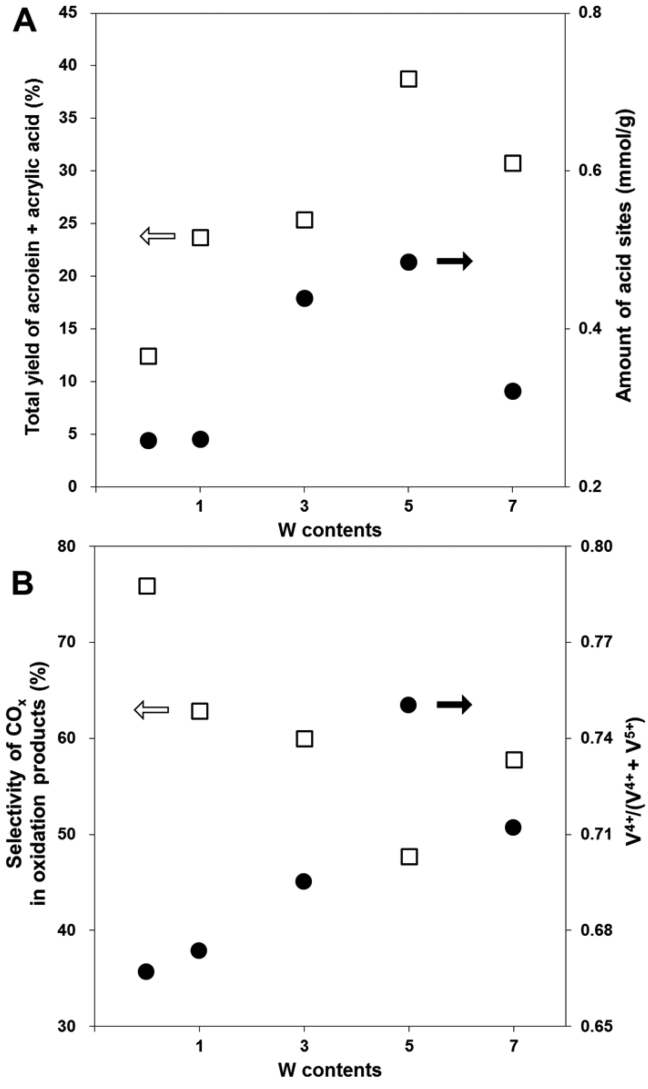

Figure 11. Correlations of (A) total yield of acrolein and acrylic acid with amount of acid sites and (B) selectivity of CO and CO_2 in oxidization products with surface ratio of $V^{4+}/(V^{4+}+V^{5+})$ as a function of tungsten contents.

Figure 12 shows results of long-term stability tests over the MoVW-5 catalyst. At the initial point (1 h), yield of CO_x was over 40%, and the yield of acrylic acid was below 25% with the complete conversion of glycerol. With passing time, it appears that the catalyst was activated by the feed including reactants and O_2. At 14 h, the production of CO_x was decreased to ca. 36%, and the highest selectivity of acrylic acid (30.5%) was recorded. During a 110 h reaction, the complete conversion of

dx.doi.org/10.1021/cs501307v | ACS Catal. 2015, 5, 82−94

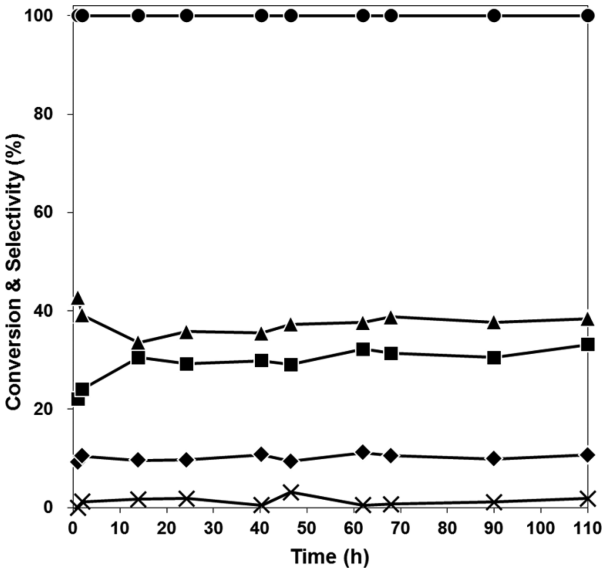

Figure 12. Long-term test of MoVW-5 in oxydehydration of glycerol: Glycerol conversion (●) and product selectivities (▲: CO + CO_2; ■: acrylic acid; ×: acrolein; and ◆: others). Reaction conditions: catalyst amount 0.3 g; reaction temperature 250 °C; total feed rate 74.34 mL min^{-1}; feed composition (vol %) glycerol/O_2/H_2O/N_2/He = 1.3/2.6/55.1/37.0/3.9. Others include acetaldehyde and acetic acid.

glycerol and high acrylic acid yield (above 30%) were maintained. The total amount of acrolein and acrylic acid remained unchanged during the test, which could mean that no severe deactivation of acid sites had occurred. This stable behavior of MoVW-5 was contributed to high coke resistance due to its low acid strength[17] and stabilization of the oxidation states of vanadium by the presence of tungsten species.

3.7. Comparative Activity Test in Two-Bed System. To demonstrate the potential of MoVW catalysts in practical applications, we performed catalytic tests with an additional acid catalyst bed. The two-bed system was formed by laying conventional acid catalyst (HZSM-5, Si/Al = 40) on MoV and MoVW-5 catalysts. This system was proven to be effective for maximizing acrylic acid production because the undesirable oxidation of glycerol can be avoided by the complete conversion of glycerol over the first bed.[8] The results are listed in Table 6. Separate sequential beds of HZSM-5 and MoV catalysts gave a 100% glycerol conversion and a 32.4% selectivity for acrylic acid. This is comparable to the value obtained for the MoVW-5 single-bed system. Interestingly, in the HZSM-5 and MoVW-5 catalyst-bed systems, much higher selectivity for acrylic acid (47.2%) was obtained with the full conversion of glycerol. This performance was also confirmed to be higher than previous results in which a two-layered system was used.[8] In addition, a remarkably low selectivity for CO and CO_2 was found compared to MoV-based system, indicating that the MoVW-5 catalyst is more selective for the conversion of acrolein to acrylic acid than the MoV catalyst. When the outstanding stability and selectivity for acrylic acid of the MoVW catalyst system are taken into consideration, we conclude that MoVW catalysts have potential for use in practical applications.

4. CONCLUSIONS

Using DFT calculations, tungsten-incorporated molybdenum vanadium mixed oxide catalysts were designed and used to gain insights into the effect of incorporated tungsten. The findings revealed that incorporated tungsten atoms induce neighboring atoms, such as molybdenum, vanadium, and oxygen, to adopt a reduced state (Mo^{5+} and V^{4+}) and more nucleophilic (oxygen), which are required properties for the selective production of acrylic acid. After confirming this, we successfully prepared the MoVW catalysts with structures similar to the computational models, which was confirmed by experimental characterizations (XRD, XANES, FT-IR, and Raman spectroscopies). XPS studies of the MoVW catalysts were in good agreement with the DFT calculation, demonstrating the validity of the models. NH_3-TPD data indicate that the presence of tungsten in the MoV structure causes an enhancement in both the amount and strength of the acid, thus facilitating dehydration of glycerol to acrolein. The incorporated tungsten species also improve the reducibility of the MoVW catalyst, making the release of lattice oxygen easier. Accordingly, this change in the oxidation state of molybdenum and vanadium as well as the reducibility promote the selective and stable conversion of acrolein to acrylic acid. Therefore, the MoVW catalysts exhibit much higher selectivity (MoVW-5; 30.5%) for acrylic acid than the MoV catalyst (12.4%) and a high stability for periods of operation of up to 110 h. The combination of the characterization results with the catalytic reaction results suggests that a weak-medium acidity and the stabilization of low oxidation state for vanadium induced by the presence of tungsten are main reasons for highly stable production of acrylic acid. A two-bed catalytic system including HZSM-5 and MoVW-5 layers exhibited remarkable selectivity (47.2%) for acrylic acid. This report not only shows a high potential for industrial applications of MoVW catalysts but also provides a foundation stone for designing bifunctional catalysts for oxydehydration of glycerol by theoretical studies.

■ ASSOCIATED CONTENT

Supporting Information

The following file is available free of charge on the ACS Publications website at DOI: 10.1021/cs501307v.

Details for modeling MoVW, calculation models of MoV and MoVW catalysts, calculated charge density differences of MoVW-3 and MoVW-7, UV−vis spectra of

Table 6. Comparative Conversion and Selectivities of Two Separate Bed Systems with HZSM (1st Layer), and MoV and MoVW-5 Catalysts (2nd Layer)[a]

		selectivity (%)				
catalyst	glycerol conversion (%)	acrylic acid	acrolein	acetic acid	CO_x	acetaldehyde
HZSM-5 + MoV	100	32.4	0.0	10.3	55.6	<1.0
HZSM-5 + MoVW-5	100	47.2	0.3	9.8	39.4	<1.0

[a]Reaction conditions: reaction temperature 250 °C; total feed rate 74.34 mL min^{-1}; feed composition (vol %) glycerol/O_2/H_2O/N_2/He = 1.3/2.6/55.1/37.0/3.9. The reaction results were taken after 2 h time-on-stream. Two layer catalyst system: first layer: HZSM-5 (0.05g); second layer: MoV or MoVW-5 catalyst (0.3 g).

dx.doi.org/10.1021/cs501307v | ACS Catal. 2015, 5, 82−94

MoV and MoVW precursor solutions, TEM images of WO_3, FT-IR and Raman spectra of MoV and MoVW catalysts, calculated insertion energy of tungsten species in MoV, MoVW-1, and MoVW-3 models, and formation energy and probability for various configuration of MoVW models (PDF)

AUTHOR INFORMATION

Corresponding Author

*E-mail: jyi@snu.ac.kr. Tel:+82-2-880-7438.

Notes

The authors declare no competing financial interest.

ACKNOWLEDGMENTS

This research is supported by Korea Ministry of Environment as "Converging technology project (202-091-001)". This work was also supported by the Supercomputing Center/Korea Institute of Science and Technology Information with supercomputing resources including technical support (KSC-2013-814 C1-025). This work was also supported by the National Research Foundation of Korea (NRF) grant funded by the Korea government (MEST) (No. 2013R1A2A2A01067164).

REFERENCES

(1) Crespo-Quesada, M.; Cárdenas-Lizana, F.; Dessimoz, A.-L.; Kiwi-Minsker, L. *ACS Catal.* **2012**, *2*, 1773−1786.
(2) Okuhara, T. *Chem. Rev.* **2002**, *102*, 3641−3666.
(3) Su, F.; Guo, Y. *Green Chem.* **2014**, *16*, 2934−2957.
(4) Alonso, D. M.; Bond, S. Q.; Dumesic, J. A. *Green. Chem.* **2010**, *12*, 1493−1513.
(5) Smith, B.; Greenwell, H. C.; Whiting, A. *Energy Env. Sci.* **2009**, *2*, 262−271.
(6) Kuchonthara, P.; Puttasawat, B.; Piumsomboon, P.; Mekasut, L.; Vitidsant, T. *Korean J. Chem. Eng.* **2012**, *29*, 1525−1530.
(7) Park, D. S.; Yun, D.; Kim, T. Y.; Baek, J.; Yun, Y. S.; Yi, J. *ChemSusChem* **2013**, *6*, 2281−2289.
(8) Witsuthammakul, A.; Sooknoi, T. *Appl. Catal., A* **2012**, *413*−*414*, 109−116.
(9) Feng, X.; Sun, B.; Yao, Y.; Su, Q.; Ji, W.; Au, C.-T. *J. Catal.* **2014**, *314*, 132−141.
(10) Kampe, P.; Giebeler, L.; Samuelis, D.; Kunert, J.; Drochner, A.; Haaß, F.; Adams, A. H.; Ott, J.; Endres, S.; Schimanke, G.; Buhrmester, T.; Martin, M.; Fuess, H.; Vogel, H. *Phys. Chem. Chem. Phys.* **2007**, *9*, 3577−3589.
(11) Xu, W.; Liu, X.; Ren, J.; Zhang, P.; Wang, Y.; Guo, Y.; Lu, G. *Catal. Commun.* **2010**, *11*, 721−726.
(12) Thadani, A. N.; Rawal, V. H. *Org. Lett.* **2002**, *4*, 4321−4323.
(13) Arntz, D.; Fischer, A.; Hopp, M.; Jacobi, S.; Sauer, J.; Ohara, T.; Sato, T.; Shimizu, N.; Schwind, H. *Ullmann's Encyclopedia of Industrial Chemistry*; Wiley-VCH: Weinheim, 2007; Vol. *1*; pp 329−346.
(14) Sithambaram, S.; Kumar, R.; Son, Y.-C.; Suib, S. L. *J. Catal.* **2008**, *253*, 269−277.
(15) Giebeler, L.; Wirth, A.; Martens, J. A.; Vogel, H.; Fuess, H. *Appl. Catal., A* **2010**, *379*, 155−165.
(16) Sadakane, M.; Endo, K.; Kodato, K.; Ishikawa, S.; Murayama, T.; Ueda, W. *Eur. J. Inorg. Chem.* **2013**, 1731−1736.
(17) Chai, S.-H.; Wang, H.-P.; Liang, Y.; Xu, B.-Q. *Green. Chem.* **2007**, *9*, 1130−1136.
(18) Mars, P.; van Krevelen, D. W. *Chem. Eng. Sci.* **1954**, *3*, 41−59.
(19) Anderson, A. B.; Ewing, D. W.; Kim, Y.; Graselli, R. K.; Durrington, J. D.; Brazdil, J. F. *J. Catal.* **1985**, *96*, 222−233.
(20) Andrushkevich, T. V.; Popova, G. Y. *Russ. Chem. Rev.* **1991**, *60*, 1023−1034.
(21) Wagner, J. B.; Su, D. S.; Schunk, S. A.; Hibst, H.; Petzoldt, J.; Schlögl, R. *J. Catal.* **2004**, *224*, 28−35.
(22) Ozka, U. S.; Watson, R. B. *Catal. Today* **2005**, *100*, 101−114.
(23) Tichý, J. *Appl. Catal., A* **1997**, *157*, 363−385.
(24) Wang, F.; Dubois, J.-L.; Ueda, W. *J. Catal.* **2009**, *268*, 260−267.
(25) Deleplanque, J.; Dubois, J.-L.; Devaux, J.-F.; Ueda, W. *Catal. Today* **2010**, *157*, 351−358.
(26) Soriano, M. D.; Concepción, P.; Nieto, J. M. L.; Cavani, F.; Guidetti, S.; Trevisanut, C. *Green Chem.* **2011**, *13*, 2954−2962.
(27) Chieregato, A.; Basile, F.; Concepción, P.; Guidetti, S.; Liosi, G.; Soriano, M. D.; Trevisanut, C.; Canani, F.; Nieto, J. M. L. *Catal. Today* **2012**, *197*, 58−65.
(28) Pestana, C. F. M.; Guerra, A. C. O.; Ferreira, G. B.; Turci, C. C.; Mota, C. J. A. *J. Braz. Chem. Soc.* **2013**, *24*, 100−105.
(29) Omata, K.; Matsumoto, K.; Murayama, T.; Ueda, W. *Chem. Lett.* **2014**, *43*, 435−437.
(30) Huang, K.; Zhan, X.-L.; Chen, F.-Q.; Lü, D.-W. *Chem. Eng. Sci.* **2003**, *58*, 81−87.
(31) Mayernick, A. D.; Janik, M. J. *J. Catal.* **2011**, *278*, 16−25.
(32) Kaukonen, M.; Krasheninnikov, A. V.; Kauppinen, E.; Nieminen, R. M. *ACS Catal.* **2013**, *3*, 159−165.
(33) Yun, D.; Kim, T. Y.; Park, D. S.; Yun, Y. S.; Han, J. W.; Yi, J. *ChemSusChem* **2014**, *7*, 2193−2201.
(34) Greeley, J.; Jaramillo, T. F.; Bonde, J.; Chorkendorff, I.; Nørskov, J. K. *Nat. Mater.* **2006**, *5*, 909−913.
(35) Studt, F.; Sharafutdinov, I.; Abild-Pedersen, F.; Elkjær, C. F.; Hummelshøj, J. S.; Dahl, S.; Chorkendorff, I.; Nørskov, J. K. *Nat. Chem.* **2014**, *6*, 320−324.
(36) Studt, F.; Abild-Pedersen, F.; Wu, Q.; Jensen, A. D.; Temel, B.; Grunwaldt, J.-D.; Nørskov, J. K. *J. Catal.* **2012**, *293*, 51−60.
(37) Nørskov, J. K.; Bligaard, T.; Rossmeisl, J.; Christensen, C. H. *Nat. Chem.* **2009**, *1*, 37−46.
(38) Ulgen, A.; Hoelderich, W. *Catal. Lett.* **2009**, *131*, 122−128.
(39) Sadakane, M.; Watanabe, N.; Katou, T.; Nodasaka, Y.; Ueda, W. *Angew. Chem.* **2007**, *119*, 1515−1518.
(40) Ravel, B.; Newville, M. *J. Synchrotron Rad.* **2005**, *12*, 537−541.
(41) Häggblad, R.; Wagner, J. B.; Deniau, B.; Millet, J.-M. M.; Holmberg, J.; Grasselli, R. K.; Hansen, S.; Andersson, A. *Top. Catal.* **2008**, *50*, 52−65.
(42) Xu, Y.; Huang, W.; Shi, Q.; Zhang, Y.; Song, L.; Zhang, Y. *J. Sol-Gel Sci. Technol.* **2012**, *64*, 493−499.
(43) Jing, F.; Katryniok, B.; Dumeignil, F.; Bordes-Richard, E.; Paul, S. *J. Catal.* **2014**, *309*, 121−135.
(44) Cortés-Jácome, M. A.; Angele-Chavez, C.; López-Salinas, E.; Navarrete, J.; Toribio, P.; Toledo, J. A. *Appl. Catal., A* **2007**, *318*, 178−189.
(45) Kresse, G.; Furthmuller, J. *Phys. Rev. B* **1996**, *54*, 11169−11186.
(46) Perdew, J. P.; Burke, K.; Ernzerhof, M. *Phys. Rev. Lett.* **1996**, *77*, 3865−3868.
(47) Blöchl, P. E. *Phys. Rev. B* **1994**, *50*, 17953−17979.
(48) Bader, R. F. W.*Atoms in Molecules: A Quantum Theory*; Oxford University Press: Oxford, 1990.
(49) Liu, W.; Xu, S.; Li, C.; Yuan, G. *Diamond. Relat. Mater.* **2012**, *29*, 59−62.
(50) Kang, J.; Hirata, A.; Kang, L.; Zhang, X.; Hou, Y.; Chen, L.; Li, C.; Fujita, T.; Akagi, K.; Chen, M. *Angew. Chem.* **2013**, *52*, 1664−1667.
(51) Shen, L.; Yin, H.; Wang, A.; Lu, X.; Zhang, C. *Chem. Eng. J.* **2014**, *244*, 168−177.
(52) Drochner, A.; Kampe, P.; Kunert, J.; Ott, J.; Vogel, H. *Appl. Catal., A* **2005**, *289*, 74−83.
(53) Botar, B.; Kögerler, P.; Hill, C. L. *Chem. Commun.* **2005**, 3138−3140.
(54) Konya, T.; Katou, T.; Murayama, T.; Ishikawa, S.; Sadakane, M.; Buttrey, D.; Ueda, W. *Catal. Sci. Technol.* **2013**, *3*, 380−387.
(55) Katou, T.; Vitry, D.; Ueda, W. *Chem. Lett.* **2003**, *32*, 1028−1029.
(56) Ueda, W.; Chen, N. F.; Oshihara, K. *Chem. Commun.* **1999**, 517−518.
(57) Vernardou, D.; Drosos, H.; Spanakis, E.; Koudoumas, E.; Savvvakis, C.; Katsarakis, N. *J. Mater. Chem.* **2011**, *21*, 513−517.
(58) Yamazoe, S.; Hitomi, Y.; Shishido, T.; Tanaka, T. *J. Phys. Chem. C* **2008**, *112*, 6869−6879.

(59) Chen, K.; Bell, A. T.; Iglesia, E. *J. Phys. Chem. B* **2000**, *104*, 1292−1299.
(60) Kunert, J.; Brochner, A.; Ott, J.; Vogel, H.; Fueß, H. *Appl. Catal., A* **2004**, *269*, 53−61.
(61) Yang, Y.-H.; Wang, Y. Y.; Ko, A.-N. *J. Porous Mater.* **2011**, *18*, 735−742.
(62) Ke, J.; Xiao, J.-W.; Zhu, W.; Liu, H.; Si, R.; Zhang, Y.-W.; Yan, C.-H. *J. Am. Chem. Soc.* **2013**, *135*, 15191−15200.
(63) Ruth, K.; Kieffer, R.; Burch, R. *J. Catal.* **1998**, *175*, 27−39.
(64) Chieregato, A.; Soriano, M. D.; Basile, F.; Liosi, G.; Zamora, S.; Concepción, P.; Cavani, F. *Appl. Catal., B* **2014**, *150−151*, 37−46.
(65) Suprun, W.; Lutecki, M.; Haber, T.; Papp, H. *J. Mol. Catal. A* **2009**, *309*, 71−78.
(66) Kim, Y. T.; Jung, K.-D.; Park, E. D. *Appl. Catal., A* **2011**, *393*, 275−287.
(67) Ueda, W.; Vitry, D.; Katou, T. *Catal. Today* **2004**, *96*, 235−240.